Al-Manar Journal of Medical and Applied Sciences (MJMAS) 01 (1): 20-33, 2025
Doi:

Type of the Paper (Article) Open Access

Pharmacological and Computational Assessment of Co(II), Cu(II), Ni(II), and Zn(II) Schiff Base Complexes: Anticancer, Antioxidant, and Antibacterial Investigations

Yahya Saber E. Mansour[1]* Nusieba A Mohammed Ibrahim[1], Saleh Bufarwa[2]

[1]*Department of Pharmacology and Toxicology, Faculty of Pharmacy, Omar Al- Mukhtar University, El-Beida Libya*
[2]*Department of chemistry, faculty of science Omar Al- Mukhtar university, El-Beida Libya*

Corresponding email. *Yahya.saber@omu.edu.ly*

Keywords:
Mixed ligand complexes, DFT calculations, Cytotoxicity, Hepatoprotective.

A B S T R A C T

Four novel mixed-ligand complexes, [Co(L1)(L2)(H2O)], [Cu(L1) (L2)(H2O)], [Ni(L1)(L2)(H2O)] and [Zn(L1)(L2)(H2O)] (L1 = Schiff base [5-(diethylamino)-2-(((4-phenylthiazol-2-yl)imino)methyl)phenol], L2 = proline have been prepared and identified. The synthesized complexes are characterized by molar conductance, magnetic measurements (μeff), elemental analysis (CHN), FTIR, UV–visible, ^{1}H NMR, ESR, mass spectrometry, and TG analysis. FTIR data are supported by density functional theory (DFT) calculations. The vibrational frequencies of molecules were computed using optimized geometries performed using DFT calculations. In terms of antibacterial activity, complexes outperform mixed ligand. Anticancer activity was screened against human cancer cells such as Follicular Thyroid Cancer cells (FTC-133). The results indicate that complexes show increased cytotoxicity in the proliferation of cell lines. Antioxidant activities were shown that mixed ligand complexes have high reactivity. Antioxidant activity determines the compounds' effect on Liver Function Enzyme (GOT, GPT, and ALP) in Sera of carbon tetrachloride-treated Albino Male Mice. Molecular docking

Introduction

Schiff bases are weak bases that can be broken down by mineral acids but not by water-based alkalis. Schiff bases made from formaldehyde tend to become polymerized [1]. Schiff bases should have functional groups close enough to the condensation site to make a five- or six-membered chelate ring when they react with metal ions [2]. The size of the formed chelate ring can be changed by moving donor atoms and groups to see how substitution and steric factors affect ring size [3]. These products have been used a lot in theoretical studies and as a starting point for the following steps to making a heterocyclic compound [4]. Those containing Schiff bases are recognized to exhibit distinctive properties [5, 6]. In biological flu-ids, where millions of possible ligands compete for metal ions in vivo [3], mixed ligand complexes play an important role in biological chemistry [7]. The Schiff bases are stable; however, the Schiff base formed from aromatic chemicals is more stable than the Schiff base derived from aliphatic components [8]. Aromatic aldehydes with efficient conjugation are more stable than aliphatic aldehydes, which are easily polymerized [9]. In addition to their anticancer characteristics [10], several mixed amino acid complexes promote the infusibility of other complexes and enhance their biological action within cells [11]. In re-cent years, such methods have become increasingly common in the chemotherapy field [12]. The synthesis and characterization of the complexes [Co(L1)(L2)(H2O)2], [Cu(L1) (L2)(H2O)2], [Ni(L1)(L2)(H2O)2], and [Zn(L1)(L2)(H2O)2] are described in this work. Density functional theory (DFT) calculations, including geometry optimization, vibrational frequency analysis, and electronic structures were reported for synthesized molecules using B3LYP functional using 6-31+G(d,p) basis set for C, H, O, N, S atoms and LANL2DZ basis set for metal atoms. In this work, we preparation of L1 [5-(diethylamino)-2-(((4-phenylthiazol-2-yl) imino) methyl) phenol] by condensation of 4-(diethylamino)-2-hydroxybenzaldehyde with 4-phenylthiazol-2-

amine. These chemicals (L1) have an orange result. The general procedure for the preparation of complexes, the general process for synthesizing complexes is by utilizing the proper amounts of substances in the molar ratio (1:1:1) (M: L1:L2). First, an ethanolic solution of L1 (2 mM) was added to an aqueous solution of metal salts Co(II), Ni(II), Zn(II)or Cu(II) (1 mM), followed by the addition of L2 (1 mM). At 35°C, the mixture was constantly agitated, and precipitates were obtained instantly. Next, the products were filtered, washed with ethanol, re-crystallized from ethanol, and dried at 60°C. Table 1 lists the physical parameters of prepared complexes. An MTT assay was used to test anticancer efficacy of L1, L2, and their complexes against FTC-133.

Materials and Methods

Experimental

Chemicals

To conduct the current research, used high-purity analytical-grade reagents in experiments. The following chemicals were utilized: 4-diethylaminosalicylaldehyde (98%, Aldrich), 2,3-diaminophenazine (90%, Aldrich), cobalt nitrate hexahydrate (98%, Fluka), nickel nitrate hexahydrate (98.5%, Fluka), copper nitrate trihydrate (99%, Aldrich), cadmium nitrate tetrahydrate (98%, Aldrich), dimethyl sulfoxide (99%, Ficher), N,N-dimethyl formamide (99.9%, Merck), methanol anhydrous (99.8%, Aldrich), and ethanol (99.8%, Fluka).

Apparatus

Molar conductivity measurements were carried out of solid complexes in dimethylformamide (DMF) solution at room temperature by using a Jenway 4510 conductivity meter. The Faraday method (Faraday balance) was used to measure magnetic susceptibility at room temperature. a PerkinElmer 2400 CHN analyzer performed elemental analyses. The metallic content of the complexes using an atomic absorption spectrometer from Thermo Scientific iCE 3300 AA Spectrometer and Auto-Sampler Module. Using FT-IR Thermo Scientific 6700 and a KBr disc to record the FT-IR spectra. The electronic spectra of the complexes were obtained by a Beckman Coulter DU 800 spectrometer, 1 cm quartz cells, and dimethylsulfoxide (DMSO) as the solvent. Mass spectra of the complexes were performed by the direct input unit (DI-50) in the Shimadzu QP-5050 GC-MS. 1HNMR spectra were carried out by Varian Gemini 200 MHz with DMSO-d*6* as the solvent. The micro-analytical team at Cairo University in Giza, Egypt conducted most of the analysis.

Synthesis of Schiff base [5-(diethylamino)-2-(((4-phenylthiazol-2-yl)imino)methyl)phenol] (L1)

L1 was prepared by 4-diethylaminosalicyaldehyde (0.97 g, 5 mmol) was added to 25 mL of hot methanol, followed by the addition of 2-amino-4-phenylthiazole (0.89 g, 5 mmol) dissolved in 25 mL of methanol (Scheme 1) [24, 25]. The mixture was refluxed for 3 hrs. After condensation, the mixture was left to cool down to room temperature, resulting in the formation of orange precipitated crystals. The crystals were then isolated by filtration.

Characterization of L1: color: orange; yield: 76%; M.p: 86 ^{o}C; elemental analysis, M.wt: 351.47 g.mol^{-1} ($C_{20}H_{21}N_3OS$) calculated: C, 72.83%; H, 6.47%; N, 14.99%; found: C, 72.80%; H, 6.40%; N, 5.05%. FT-IR (KBr, cm^{-1}): 3047 υ(C-H)arm; 3359 υ(O-H); 1244 υ(C-N)phe; 1610 υ(C=N)azo; 1025 υ(C-O). ^{1}HNMR (300 MHz, DMSO-*d6*) δ 13.46 (m, 1H, OH), δ 13.36 (m, 1H, OH), δ 8.62 (m, 2H, CH=N), δ 8.52 (dd, J = 6.2, 3.4 Hz, 2H, Ar-H), δ 8.34 (s, 4H, Ar-H), δ 7.73 (dd, J = 6.2, 3.3 Hz, 2H, Ar-H), δ 7.38 (d, J = 2.1 Hz, 1H, Ar-H), δ 7.30 (d = 8.9 Hz, 1H, Ar-H), δ 7.09 (dd, J = 8.7, 2.2 Hz,2H, Ar-H), δ 6.89 (J = 8.7, 2.5 Hz, 2H, Ar-H), δ 4.79 (q, J = 6.9 Hz, 4H, CH_2), δ 2.49 (t, J = 7.1 Hz, 6H, CH_3).

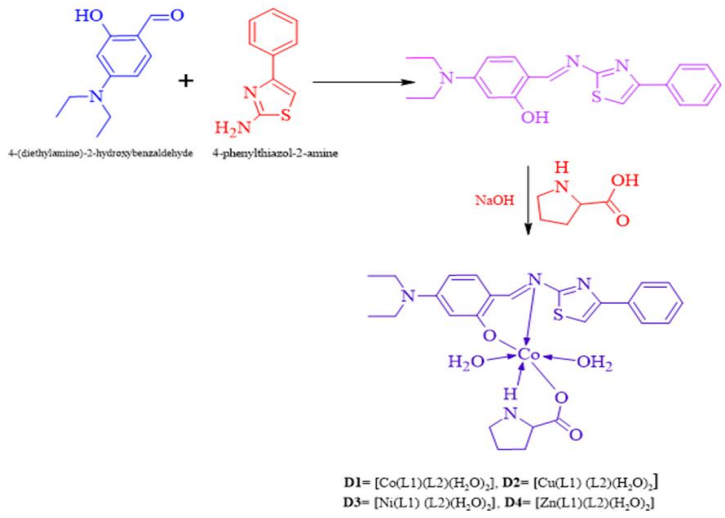

Scheme 1. *Synthesis of L1 and C1-C4 complexes.*

Synthesis of complexes: a general produce

Complexes were prepared by mixing: $CoCl_2.6H_2O$, (1.456 g, 5 mmol); $NiCl_2$ (1.454 g, 5mmol); $CuCl_2.2H_2O$ (1.208 g, 5 mmol), and $ZnCl_2.4H_2O$ (1.542g, 5mmol) with (2.803g, 5 mmol) of L1 (molar ratio 1:1) in solvent mixture DMF/EtOH/H_2O (volume ratio 10:3:3 cm3) L2 (**Scheme 1**) [24]. The mixture was refluxed for 24 hr, and prepared complexes were left to cool at room temperature, then the mixture was filtered. The abovementioned method was also used to synthesize C2-C3 solid complexes utilizing $NiCl_2$ (1.454 g, 5mmol); $CuCl_2.2H_2O$ (1.208 g, 5 mmol), and $ZnCl_2.4H_2O$ (1.542g, 5mmol), respectively. Different analytical methods were used to determine the characterization of the ligand and its complexes with metal ions. The results obtained for the metal complexes were listed and summarized as follows:

Co(II) complex (C1)

Yield 72%, color: Light blue, M.p: 188 °C, M.wt: 523.52 g.mol^{-1}, Λm:17.9 ohm^{-1}.cm^{-1}.mol^{-1}; elemental analysis for complex ($C_{25}H_{28}CoN_4O_3S$) calculated: C, 57.02 %; H, 5.11 %; N, 10.43 % ; S, 5.78 % and M, 10.86 %; found: C, 57.36 %; H, 5.39 %, N, 10.70 ; S, 6.12 % and M, 11.26 %. FT-IR (KBr cm-1): 3056 υ(C-H)arm; 1247 υ(C-O); 1618 υ(C=N); 443 υ(Co-N); 525 υ(Co-O)

2.4.2. Ni(II) Complex (C2)

Yield 70%, color: Brown, M.p: 200 °C, M.wt: 523.28 g.mol-1, Λm:17.4 ohm-1.cm-1.mol-1; elemental analysis for complex (C25H28NiN4O3S) calculated: C, 57.38 %; H, 5.39 %; N, 10.71 %; S, 5.13 % and M, 11.06 %; found: C, 57.38 %; H, 5.39 %, N, 10.71 %; S, 6.13 % and M, 11.22 %. FT-IR (KBr cm-1): 3047 υ(C-H)arm; 1258 υ(C-O); 1618 υ(C=N); 441 υ(Ni-N); 526 υ(Ni-O).

2.4.3. Cu(II) Complex (C3)

Yield 73%, color: dark brown, M.p: 188 °C, M.wt: 622.23 g.mol^{-1}, Λm: 16.8 ohm^{-1}.cm^{-1}.mol^{-1}; elemental analysis for complex ($C_{34}H_{34}CuN_6O_2$) calculated: C, 65.63 %; H, 5.51 %; N, 13.51 % and M, 10.21 %; found: C, 50.95 %; H, 5.54 %, N, 13.49 % and M, 10.18 %. FT-IR (KBr cm-1): 3059 υ(C-H)arm; 1244 υ(C-O); 1619 υ(C=N); 443 υ(Cu-N); 523 υ(Cu-O).

Zn(II) Complex (C4)

Yield 78%, color: Yellow, M.p: 263 °C, M.wt: 529.96 g.mol^{-1}, Λm: 18.5 ohm^{-1}.cm^{-1}.mol^{-1}; elemental analysis for complex ($C_{25}H_{28}ZnN_4O_3S$) calculated: C, 60.85 %; H, 5.11 %; N, 12.52 % and M, 16.75 %; found: C, 56.66 %; H, 5.33 %, N, 10.57 %, S, 6.05 % and M, 12.34 %. FT-IR (KBr cm-1): 3053 υ(C-H)arm; 1245 υ(C-O); 1620 υ(C=N); 428 υ(Zn-N); 574 υ(Zn-O). ^{1}HNMR (300 MHz, DMSO-*d6*) δ 8.72 (m, 2H, CH=N), δ 8.45 (dd, J = 6.2, 3.4 Hz, 2H, Ar-H), δ 8.29 (s, 4H, Ar-H), δ 7.70 (dd, J = 6.2, 3.3 Hz, 2H, Ar-H), δ 7.37 (d, J = 2.1 Hz, 1H, ArH), δ 7.28 (d = 8.9 Hz, 1H, , Ar-H), δ 7.01 (dd, J = 8.7, 2.2 Hz,2H, Ar-H), δ 6.85 (J = 8.7, 2.5 Hz, 2H, Ar-H), δ 4.79 (q, J = 6.9 Hz, 4H, CH_2), and δ 2.49 (t, J = 7.1 Hz, 6H, CH_3).

Biological activity

Cytotoxicity assays

3-(4,5-dimethylthiazol-2-yl)-2,5-diphenyl-2H-tetrazolium bromide (MTT) cell viability assay was performed on 96-well plates to determine the substance's cytotoxicity. 1x10^4 cells were used to seed each well using cell lines. The cells were treated with the tested chemical once they had formed a confluent monolayer or after 24 hrs. After 72 hrs of treatment, the vitality of the cells was determined by removing the medium, adding 28 L of a 2 mg/mL MTT solution, and incubating the cells at 37 °C for 1.5 hours. After removing the MTT solution, the crystals in the wells were solubilized by adding 130 L of Dimethylsulfoxide (DMSO) and incubating for 15 min at 37 °C with shaking. The absorbency was determined using a microplate reader set to 490 nm (test wavelength) and repeated three times. The following equation was used to compute the rate of cell growth inhibition:

$$\textbf{Inhibition rate} = \frac{A-B}{A} * 100$$

Where A and B are the optical density of the control and the optical density of the test.

Assessment of Hepatoprotective and kidney protective effects

Hepatoprotective and kidney protective effects were assessed in mice treated with complexes. The parameters of assessment were assessed in liver fiction enzymes (GOT), (GPT) and (AlP) in serum, in addition to kidney function test (Urea, Creatinine).

Experimental design

The dose (200 mg/kg) was tested for hepatoprotective and kidney protective effects in eight groups of mice in a hepatoprotective and kidney protective study (each of 4 mice, and the total was 32 animals):

Group I: For 7 days, mice were given a single daily dose (0.1 ml) of distilled water (negative control (DW)).

Group II: Mice received a single daily dose (0.1 ml) of DMSO (positive control (DMSO)) for 7 days.

Group III: Mice were given a single dose of 0.2 % CCl_4 in olive oil (0.1 ml) for 1 day and then Cu, Ni, and Zn complexes (0.1 ml) once daily for the next 7 days.

The tested compounds were IP injected for eight days, and the mice were killed and dissected. Before the mouse was sacrificed, blood was taken through heart puncture, transferred to an Eppendorf tube, and allowed to clot at room temperature for 15 minutes before serum was extracted using centrifugation at 3000 rpm for 10 minutes. The serum was used for the assessment of liver fiction test (GOT), (GPT) and (Alp), and (Urea, Creatinine test).

(GOT): GOT enzyme activity was measured in mouse serum using an enzymatic colorimetric technique. A commercial kit (Randox Company) was employed for this purpose.

(GPT): The enzyme activity of ALT was evaluated in mouse serum using the same enzymatic colorimetric approach used to determine AST's activity using a commercial kit (Randox Company).
(ALP): The enzyme ALP was measured in mouse serum using a commercial kit manufactured by Bio Merieux Company and the most generally used method. Di-sodium phenyl phosphate is hydrolyzed, resulting in the liberation of phenol and the creation of sodium phosphate. The amount of phenol produced is calculated using calorimetry.

Computational Methods

The electronic structure calculations were carried out using the Gaussian-16 (G16) quantum chemistry package [13]. Normal-mode analysis of frequencies was counted for all structures to ensure imaginary frequencies' absence in the minima [14- 16]. Using Becke's three-parameter hybrid method, the calculations were carried out using the LYP correlation functional (B3LYP) [17]. The geometry optimization was performed using B3LYP functionals and 31+G(d,p) basis set for C, H, O, N, and S atoms and the LANL2DZ basis set [18] for metal atoms. The solvent effects have a significant impact by utilizing the conductor-like polarizable continuum model (CPCM) method with DMSO as solvent. Frequency calculations were performed on the optimized geometries at the same level of theory; all computed vibrational transitions have no imaginary frequency implying that each optimized geometry is located at the global minimum point on the potential energy surface. The calculated vibrational modes in the absence of the imaginary frequencies indicate that the molecule's corresponding optimized structure is the most stable one. The DFT calculations obtained vibrational mode values that were measured by a factor of 0.966 [19]. The frontiers' molecular orbitals energies and electron densities were calculated using the B3LYP method and the LANL2DZ as a basis set. The HOMO-LUMO energy calculations were measured for all compounds at the same level of theory using the TD-DFT (Time-Dependent Density Functional Theory) method [20].

RESULTS

Synthesis and Characterization

Several experimental techniques such as FT-IR, ^{1}H NMR, UV-Vis.MS, elemental analysis, molar conductance, and magnetic measurements were performed to analyze L1, L2, and their complexes [5]. Furthermore, geometry optimization has been performed using a conjugate gradient method.

Molar Conductance Measurements

Electrolytic complexes are shown by the molar conductance values for the complexes in DMSO at 10^{-3} M at 25°C. Furthermore, the data suggest that ions exist outside the coordination circles, as given in Table 1 [6]. Molar conductance values for complexes confirmed non-electrolyte.

Mass spectrometry

The mass spectrometry analysis revealed m/z values of 617.2, 616.2, 621.2, and 672.1 for the molecular ion peaks of metal complexes C1, C2, C3, and C4, respectively. These results are deemed reasonable and consistent with the molecular structures of complexes.

Table 1. Physical data of the ligands and mixed ligand complexes.

Compounds	M.F.	M.Wt	m/z	Yield %	color	Mp	Elemental analysis (% found) % cal				
							C	H	N	S	M
L_1	$C_{20}H_{21}N_3OS$	351.47	-	76	orange	86	67.87 (68.35)	5.65 (6.02)	11.65 (11.96)	8.65 (9.12)	-
L_2	$C_5H_9NO_2$	115.13	-	-	White	223	-	-	-	-	-
C_1	$C_{25}H_{32}CoN_4O_5S$	559.53	617.2	72	Light blue	188	57.02 (57.36)	5.11 (5.39)	10.43 (10.70)	5.78 (6.12)	10.86 (11.26)
C_2	$C_{25}H_{32}N_4NiO_5S$	559.29	616.2	70	Brown	200	57.38 (57.38)	5.39 (5.39)	10.71 (10.71)	5.13 (6.13)	11.06 (11.22)
C_3	$C_{25}H_{32}CuN_4O_5S$	564.15	621.2	67	Light green	240	55.88 (56.21)	5.07 (5.22)	10.09 (10.30)	6.11 (5.88)	11.87 (12.03)
C_4	$C_{25}H_{32}ZnN_4O_5S$	565.98	672.1	78	Yellow	263	56.33 (56.66)	5.56 (5.33)	10.87 (10.57)	6.21 (6.05)	12.20 (12.34)

FTIR spectral studies

FT-IR spectra of L1 and L2 show broad bands at 3359 and 3345 cm^{-1}, which were assigned to υ(O-H) of COOH and phenolic (Table 2). These bands in metal complexes disappeared and appeared two strong bands in spectra of complexes at 1632–1577 and 1385–1370 cm^{-1} were assigned to asymmetric and symmetric stretching frequencies of the carboxylate group, with a difference >200 cm^{-1} verified a monodentate type for carboxylate

group. In spectra of L1 and L2, bands observed at 1610 and 3429 cm^{-1} can be assigned to υ(C=N) of the azomethine group and υ(N-H), on complexation, these bands were shifted to higher and lower frequencies indicating involvement in chelation. The spectra are additionally distinguished by the presence of a novel band in the range of 432-472 cm^{-1} attributed to (M-N), showing the presence of nitrogen atoms in conjunction with metallic ions [9]. The coordination of metal ion through O- atom was further confirmed by forming a medium new band at 512-556 cm-1 ascribed to (M-O) [10]. These findings are pretty consistent with the figures published previously [11]. The coordination of the (H_2O) molecules and the M(II) ions resulted in the formation of vibrational bands in the ranges (754-712) cm^{-1} (M-OH_2) and (3343-3356) cm^{-1} attributed to OH in H_2O in all complexes [12].

Table 2: IR spectra of the ligand and its mixed ligand complexes.

Compounds	υ(O-H): COOH, phenolic, H_2O	υ(N-H)	υ(C=N)	$\nu_{as}(COO^-)$ $\nu_s(COO^-)^-$	Δν (ν_{as} - ν_s) $^-$	pH_2O	υ(M-O)	υ(M-N)
L_1	3256	-	1625	-----	-	-	-	-
	(3359)		(1610)					
L_2	3345	3429	-	1620	-			
				1406				
C_1	3386	3224	1625	1632	220	743	534	470
			1618	1412				
C_2	3343	3246	1610	1586	222	712	546	461
			1618	1364				
C_3	3416	3176	1615	1582	222	736	543	445
			1619	1360				
C_4	3356	3226	1615	1577	213	754	539	453
			1620	1364				

Table 3: The electronic absorption spectra of the ligands and their complexes

Compounds	Band positions *nm* (cm^{-1})	Assignment	$\mu_{eff.}$ (BM)	Suggested geometry
L_1	256 (41666)	(π-π*)	-----	-----
	351(31347)	(n-π*)		
L_2	243 (41666)	(π-π*)	-------	---------
	282 (35211)			
	351 (28653)	(n-π*)		
C_1	265(37735)	LF	5.64	octahedral
	318(31446)			
		$^4T_1g(F) \rightarrow {}^4T_1g(P)$		
	543(16501)	$^4T_1g(F) \rightarrow {}^4T_2g$		
C_2	264(37878)	LF	4.23	Octahedral
	318(31446)	CT		
	518(19305)	$^3A_{2g}(F) \rightarrow {}^3T_{1g}(P)$		
	826(12106)	$^3A_{2g}(F) \rightarrow {}^3T_{2g}(F)$		
C_3	264(37878)	LF	1.61	Distorted Octahedral
	318(31446)	CT		
	623(19305)	$^2B_1g \rightarrow {}^2B_2g$		
C_4	261(38314)	L.F	Dia	Octahedral
	318(31446)	C.T		

Electronic Absorption Spectra and Magnetic Moment

The optimized geometry and (TD-DFT) calculations have been used to examine the electronic absorption behaviors of the studied compound in solvent media [23-25]. In this calculation, we used B3LYP functional (exchange-correlation func-

tional [20, 21]) with the 6-31+G(d,p) basis set for C, H, O, N, and S atoms and the effective core potential LANL2DZ basis set for metal atoms. The UV-Vis spectrum of L1 was shown the intense band at 256 nm and 351 nm, which belonged to the π - π * and n$\rightarrow$ π * transitions. L2 spectrum showed two bands at 243 nm and 282 nm assigned to $\pi \rightarrow \pi$ * transition and 351 nm, whereas the third band may be assigned to the n$\rightarrow$ π * transition [26]. The cobalt (II) complex spectrum showed a prominent band at around 543 nm, assigned to the $4T_2g \rightarrow 4T_2g$ transition. This could imply that Co (II) complex has octahedral geometry. Bandwidth at 623 nm generated by the 2B1g $\rightarrow$ 2B2g transition in Cu (II) complex hints at a distorted octahedral structure [27]. The UV spectra of Ni (II) complex showed a shift in position, with two bands appearing at 674 nm and 887 nm, which were assigned to $3A_2g(F) \rightarrow 3T_1g(P)$ and $3A_2g(F) \rightarrow 3T_2g(F)$ transitions of octahedral structure [28]. The Ni (II) complex spectrum revealed a shift in the location of the CT transition and two bands at 518 nm and 826 nm, which were assigned to $4T_1g \rightarrow 4T_1g$ (P) and 4T1g$\rightarrow$ 4A2g(F) transitions, respectively. The d_{10} to Zn (II) complex spectrum reveals absorption bands at 256 nm for LF transition and 323 nm attributable to (MLCT) transition, which is comparable with octahedral complexes [29]. All data are given in Table (3).

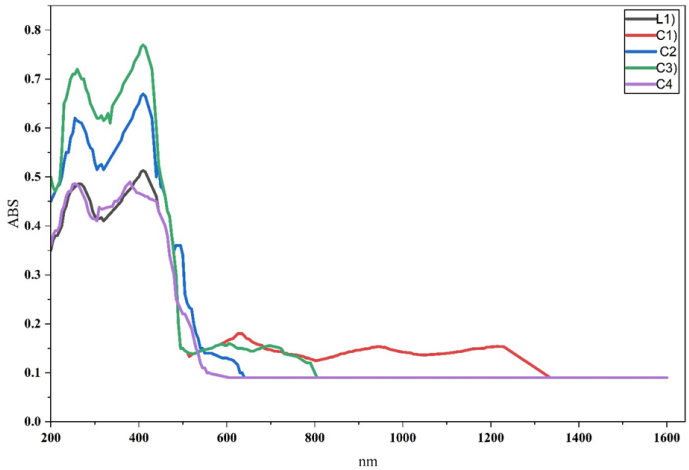

Figure 1. Electronic Absorption Spectra of the Ligands (L1) and Their Metal Complexes

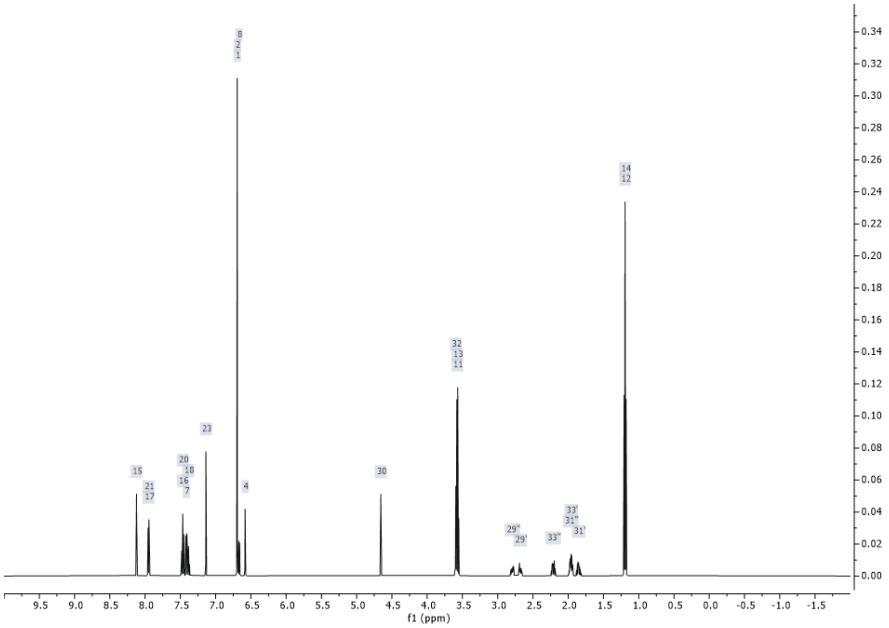

Figure 2. ^{1}H NMR Spectra of Zn Complex (C4)

^{1}H NMR spectra

^{1}H NMR spectra provide the positions of proton signals for (C4) (Figures 2). The proton signal attributed to phenol, δOH, was observed at 13.43 ppm, while the azomethine proton signal, δCH=N, appeared at 8.62 ppm [24]. In previous studies, a proton signal for the proline ligand was also recorded. Fourteen aromatic δCH protons were detected in the 4.79 ppm range, along with four aliphatic δCH_2 protons and six δCH_3 protons in the ligand. At C4, the phenol proton at δOH 13.43 and 13.46 ppm disappears as it enters the ligand in the complex. Additionally, the shift in a signal of the azomethine group of the compound suggests that the compound is formed through the nitrogen atom of azomethine.

Thermal analysis

In the current work, we conducted thermal analysis to investigate the thermal stability of complexes, synthesized during the research. The aim was to determine the presence or absence of solvent molecules, and whether they were located inside or outside the inner coordination sphere of the complex [50, 51]. The L1 and its complexes underwent thermogravimetric analysis from 0-600 °C with a heating rate of 10 °C.min^{-1}. All thermal decomposition data for the ligand and its complexes shown in (Figure 3) are listed in (Figure 3). The thermal curve pattern for the decomposition of C1, C2, and C3 complexes converges in three steps, with a slight difference in C4, which has four steps. The complexes begin to decompose in the first step at a temperature range of 218-243 °C with the loss of the two azomethine groups and part of the organic ligand. In the second step, the remaining organic ligand decomposes at 235–520 °C, leaving the metal oxide as a final product behind.

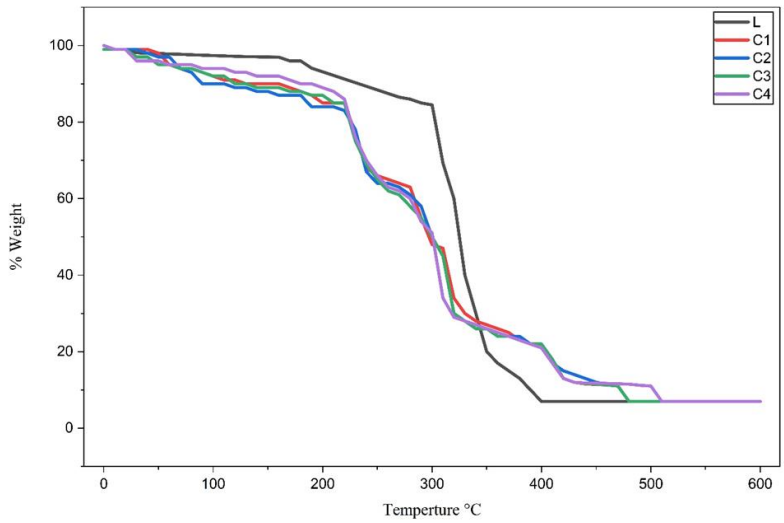

Figure 3. Thermogravimetric Analysis (TGA) and Thermal Decomposition Behavior of L1 and Its Metal Complexes (C1–C4)

The geometry optimization of the complexes

The geometry optimization of the D1-D4 complexes was obtained using the B3LYP functionals [21, 22] with the 6-31+G(d,p) basis set for C, H, O, N, S atoms and the effective core potential LANL2DZ basis set for metal atoms. The optimized structures of the C1, C2, C3, and C4 according to the B3LYP/LANL2DZ level of theory are shown in Figure 4. Table 4 displays the selected bond distances and bond angles of the optimized structures of complexes. The calculated geometries of C1, C3 and C4 indicated an octahedral environment around the central metal atom. Figure 1 supports the distorted octahedral environment around the central Cu atom. The calculated values of the C-Cu-N and O-Cu-O angles are close to 90°.

Table 4. Selected bond lengths (Å) and bond angles (°) of the computed structures of the D1-D4 complexes according to DFT calculations.

Bond Lengths (Å) of D1		Bond Lengths (Å) of D2		Bond Lengths (Å) of D3	
N51-Co46	2.734	N50-Cu66	2.199	N50-Ni66	2.198
O19-Co46	2.681	O19-Cu66	2.749	O19-Ni66	2.748
N18-Co46	2.768	N18-Cu66	2.922	N18-Ni66	3.343
O61-Co46	2.731	O60-Cu66	2.834	O60-Ni66	2.834
O64-Co46	2.726	O64-Cu66	3.203	O64-Ni66	3.203
O57-Co46	2.759	O56-Cu66	2.418	O56-Ni66	2.418
N18-C7	1.329	N18-C7	1.329	N18-C7	1.329
Angels (°) of D1		**Angels (°) of D2**		**Angels (°) of D3**	
C7-Co46-N18	117.2	C7-Cu66-N18	119.0	C7-Ni66-N18	90.7
C40-Co46-N18	113.5	C40-Cu66-N18	48.8	C40-Ni66-N18	168.7
O56-Co46-O57	112.4	O56-Cu66-O57	99.6	O55-Ni66-O56	99.6
O19-Co46-N18	67.7	O19-Cu66-N18	58.8	O19-Ni66-N18	70.4
O61-Co46-O64	86.5	O61-Cu66-O64	76.3	O60-Ni66-O63	76.2
N51-Co46-C57	49.5	N50-Cu66-C46	98.6	N50-Ni66-O56	80.7

Bond Lengths (Å) of D4		Angels (°) of D4	
N50-Zn66	2.970	C7-Zn66-N18	119.0
O19-Zn66	2.748	C40-Zn66-N18	111.4
N18-Zn66	3.343	O55-Zn66-O56	99.6
O60-Zn66	2.834	O19-Zn66-N18	58.8
O63-Zn66	3.203	O60-Zn66-O63	76.2

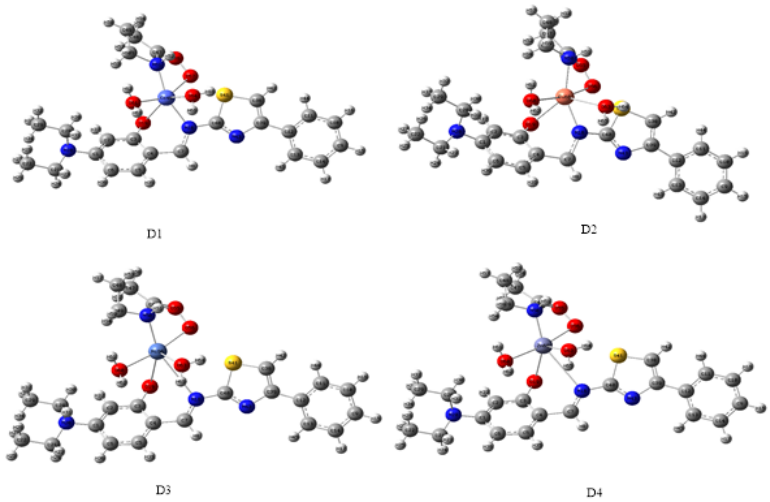

Figure 4. Optimized structures of D1, D2, D3, and D4 complexes according to DFT calculations using B3LYP functional with the 6-31+G(d, p) basis set for C, H, O, N, S atoms and LANL2DZ basis set for metals.

Electronic Structures

The calculated energies and electron densities of the frontiers molecular orbitals were performed to elucidate the electronic properties of the synthesized complexes. Figures 5 and 6 explains the energy profile of the HOMO's (highest occupied molecular orbitals), LUMO's (lowest unoccupied molecular orbitals), and HOMO-LUMO gaps for C1, C2, C3, and C4, which are calculated at the B3LYP functional with the 6-31+G(d,p) basis set for C, H, O, N, S and LANL2DZ basis set for metal atoms in DMSO as solvent. The HOMO-LUMO energies of the complexes provide general information about the stability and energetic behavior of the complexes. The chemical hardness (η) is a good indicator of chemical stability. The molecules having a large energy gap are known as hard, and small energy gaps are known as soft molecules. The hard molecules are less polarizable than the soft ones because they need large energy for excitation. In this study, the chemical potential (μ), hardness value (η), softness (S), electronegativity (x), and electrophilicity index (ω) of molecules are calculated. The HOMO-LUMO energy gap values noted that the energy values of the HOMO orbitals for all compounds are close to each other. The HOMO-LUMO energy gaps of the Cu^{2+} complex (Figure 5 are higher than Co^{2+} and Zn^{2+} complexes and very close to Ni^{2+}complexe. However, it is found that the calculated energy values of the HOMO orbitals of C1–C3, in general, are lower than that one of the corresponding Zn^{2+} complex. According to the reactivity descriptors, the values of complexes are given in Table 5. The negative values of chemical potential (μ) (−3.80, −4.48, -4.30, and −2.76 eV) show their stability means that these do not undergo decomposition into their components. As shown in Table 5, the compound with the lowest energy gap compared to the three other complexes is compound d4 (ΔEgap is 1.03 eV in DMSO), making it the softest molecule. The calculated value of chemical hardness (η), supported by the HOMO–LUMO energy gap for complexes C1, C2, C3, and C4 has been found to be: 1.47, 1.84, 1.81 and 0.52 eV, respectively (Table 5). The chemical hardness (softness) value of D4 complex is lower (greater) among all the investigated complexes in DMSO as a solvent. Hence, D4 complex is more reactive than all the complexes. It should be noted that the complex that has the lowest LUMO energy is the compound C2 (E = −2.64 eV), indicating a good electron acceptor. The electrophilicity index values (ω) for complexes (4.91, 5.45, 5.11 and 7.32 eV, respectively) related to chemical potential and hardness indicate that the C4 complex is the strongest electrophile among all complexes. However, the C2 complex has a higher electronegativity value (x = 4.48eV) than all compounds; this property may explain its superior activity in catalysis.

Table 5. Quantum chemical descriptors for complexes in DMSO.

	C1	**C2**	**C3**	**C4**
E_{HOMO} (eV)	-5.27	-6.32	-6.11	-3.27
E_{LUMO} (eV)	-2.33	-2.64	-2.49	-2.24
ΔE_{gap}(eV)	2.94	3.86	3.62	1.03
μ (eV)	-3.80	-4.48	-4.30	-2.76
η (eV)	1.47	1.84	1.81	0.52
S (eV)	0.34	0.27	0.28	0.97
X (eV)	3.80	4.48	4.30	2.76
ω (eV)	4.91	5.45	5.11	7.32

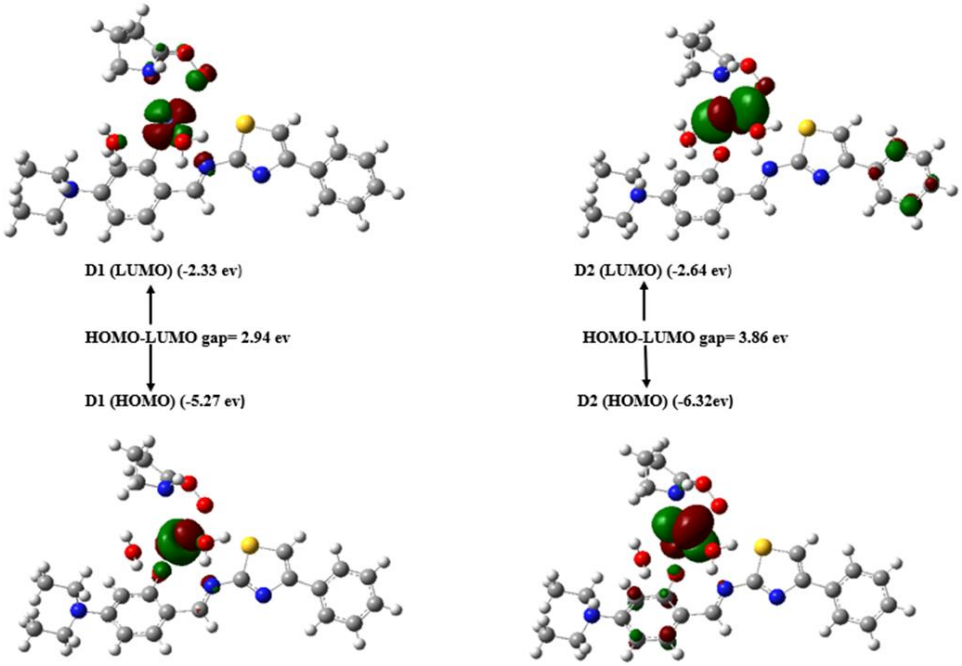

Figure 5. Energy profile of the frontier orbitals HOMO and LUMO and HOMO-LUMO gaps for C1 and C2, calculated at the B3LYP functional with the 6-31+G(d,p) basis set for C, H, O, N and S atoms and LANL2DZ basis set for Co^{+2} and Cu+2 atoms in DMSO.

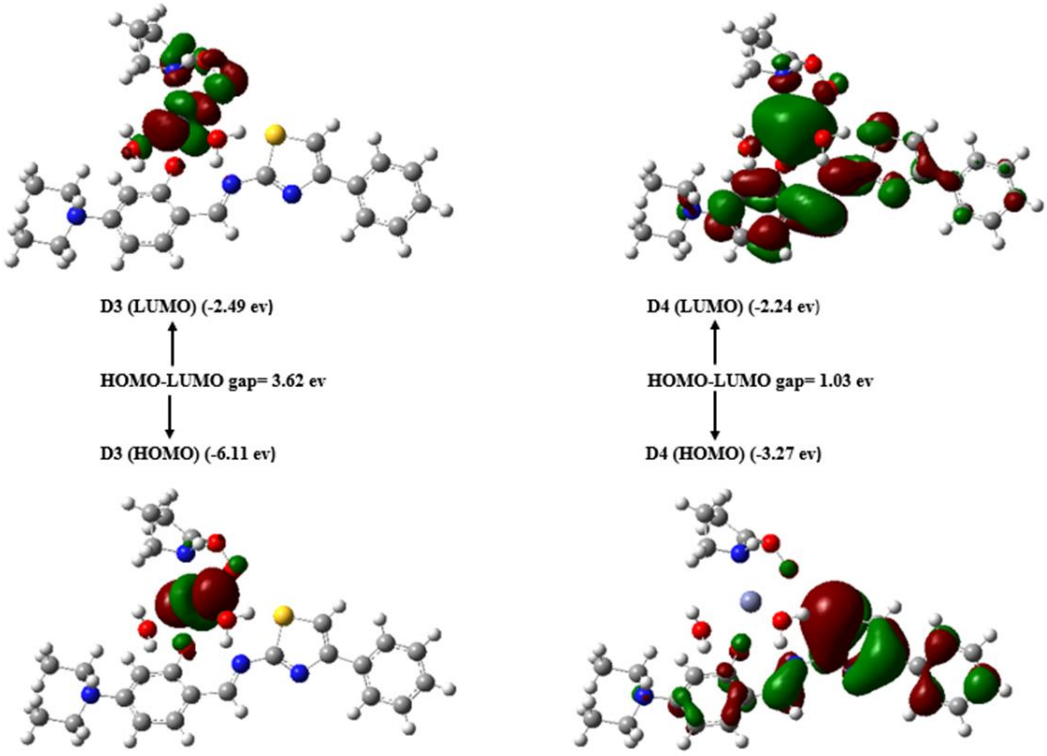

Figure 6. Energy profile of the frontier orbitals HOMO and LUMO, and HOMO-LUMO gaps for C3 and C4, calculated at the B3LYP functional with the 6-31+G (d, p) basis set for C, H, O, N and S atoms and LANL2DZ basis set for Ni^{+2} and Zn^{+2} atoms in DMSO.

Hepatoprotective Activity

In the control of physiological processes, the liver plays a crucial function. It is involved in several critical functions such as secretion, storage, and metabolism, and it was tested in mice serum for liver function enzymes (GOT, GPT, and ALP) as well as kidney function (Urea, Creatinine) [33]. GOT control mice (CCl4-treated) had an activity of 75.03± 0.81 Unit/L, GPT control mice (CCl4-treated) had an activity of 40.25±1.63 Unit/L, and ALP activity in control mice (CCl4-treated) had an activity of 92.25±5.18 Unit/L. Table 6 contains the results. The capacity of these substances extract to function as anti-oxidants through the method of down-regulating ROS, preventing DNA damage, and attenuating protein and lipid oxidation resulted in a decrease or increase of examined parameters (GPT, GOT, ALP, creatinine, urea, Alb, and Tsp) [34].

Table 6: Effect of the compounds on Liver Function Enzyme

Groups	Dose (mg/Kg)	GOT	GPT	ALP
Control(I)(D.W)	-	22.00±3.51	25.66±3.38	42.33±1.45
Control(II)(DMSO)	-	17.33±0.88	25.00±0.57	43.66±0.88
$[Co(L_1)(L_2)(H_2O)_2]$	200	10.34±0.11	17.68±0.33	30.49±1.34
$[Cu(L_1)(L_2)(H_2O)_2]$	200	21.00±1.42	27.00±1.22	31.00±1.53
$[Ni(L_1)(L_2)(H_2O)_2]$	200	36.00±1.54	49.00±0.21	60.00±0.33
$[Zn(L_1)(L_2)(H_2O)_2]$	200	32.00±1.34	46.00±0.21	58.00±0.54

Cytotoxicity Assays (Anticancer A activity)

The cytotoxic impact of the substances on Follicular Thyroid Cancer (FTC133) was determined using (MTT). Using various doses of chemicals, MTT was created to calculate cell viability and inhibition rate on a tumour cell line [35]. Compared to the normal cell line WRL-68, the percentage viability of treated cells was calculated. The cytotoxic effect of Cu(II) complex at concentrations ranging from 12.5 to 400 g/ml on FTC133 cells resulted in a decrease in cell viability (%) at 400 g/ml (60.792.85), with the highest FTC133 cell viability (95.170.94) at 12.5 g/ml. With an IC50 of 125.4 g/ml, Cu (II) complex was shown to have the most powerful cytotoxic effect [36]. The action of the chemical Cu (II) complex on the WRL-68 normal cell line yielded an IC50 of 234.3 g/ml [37, 38]. The presence of histidine, metal ions, aromatic ring, and C=N in all produced compounds made them more active, according to the data (imine group) shown in Table (7).

Table 7: Cytotoxic effect of Cu(II)complex on FTC133 and WRL-68 cells after 24 hours incubation at 37℃.

Cu(II)complex Concentrations(µg/ml)	Viable cell count of FTC133 cell line	Viable cell count of WRL-68 cell line
400	60.79±2.85	80.88±4.53
200	62.45±2.52	87.92±3.57
100	81.77±4.10	92.20±2.77
50	88.66±6.57	96.48±1.29
25	91.49±4.80	96.95±1.14
12.5	95.17±0.94	94.29±2.97

Conclusion

Four new complexes have been synthesized and characterized utilizing various physicochemical and spectroscopic techniques. UV spectroscopy and electrophoresis tests include elemental analysis, molar conductivity, magnetic susceptibility, electronic, and FT-IR spectra. The geometry of each metal is octahedral, with six coordinates. Finally, our newly synthesized Schiff base and its complexes were tested in vitro for anti-bacterial activity. The findings of this study revealed that freshly synthesized chemicals have potent anti-bacterial properties against bacterial strains. Finally, the findings of this study showed that L-proline administration at a dose of 200 mg/kg for seven days reduces hepatic lipid peroxidation caused by CCl_4 intoxication, increases the ac-

tivities of hepatic antioxidant enzymes (SOD, catalase, GR, GPx, and GST), and improves pathological liver changes, implying that L-proline is combating CCl4-induced liver hepatotoxicity. L-hepatoprotective proline's impact against CCl4-induced liver changes may be due to a combination of factors, including increased antioxidant enzyme activity, which scavenges free radicals, decreased formation of CCl_4-derived free radicals, and the anti-oxidant properties of L-proline. Finally, these findings showed that L-proline treatment had a hepatoprotective effect in mice when exposed to CCl4-induced hepatotoxicity. The DFT calculations of four novel mixed-ligand complexes synthesized C1, C2, C3, and C4 complexes have been completed for their structural determination, HOMO, LUMO study, and to calculate reactivity descriptors. The lower HOMO–LUMO energy gap value explains the kinetic stability and higher reactivity of C4 complex in comparison with the other three complexes. In addition, the electrophilicity index value ω (7.32 eV in DMSO as a solvent) indicates that the C4 complex is the strongest electrophile of all studied complexes.

Acknowledgement
We gratefully acknowledge Chemistry department, Omar Al-Mukhtar University.

ETHICS
The authors declare that there are no ethical concerns associated with this study. All data were obtained and analyzed following accepted ethical standards. The authors agree to address any ethical issues that may arise after the publication of this manuscript.

Conflicts of Interest
The authors declare no competing financial interests.

Author contributions: 1.2 developed the theoretical formalism, performed the analytic calculations and performed the numerical simulations. Both 1.2 and 2.3. authors contributed to the final version of the manuscript. 1.3. supervised the project.

Funding: No funding.

References

1. Talia, JM.; Debattista, NB.; Pappano, NB. New antimicrobial combinations: substituted chalcones-oxacillin against methicillin resistant Staphylococcus aureus. Braz J Microbiol. 2011, 42, 470–475.

2. Eumkeb, G.; Siriwong, S.; Phitaktim, S.; Rojtinnakorn, N.; Sakdarat, S. Synergistic activity and mode of action of flavonoids isolated from smaller galangal and amoxicillin combinations against amoxicillin-resistant Escherichia coli. J Appl Microbiol. 2012, 112, 55–64.

3. Do, TH.; Nguyen, DM.; Truong, VD.; Do, THT.; Le, MT.; Pham, TQ.; Thai, KM.; Tran, TD. Synthesis and selective cytotoxic activities on rhabdomyosarcoma and noncancerous cells of some heterocyclic chalcones. Molecules. 2016, 21(3), 329. doi:10.3390/molecules21030329

4. Doan, TN.; Tran, TD. Synthesis, anti-oxidant and antimicrobial activities of a novel series of chalcones, pyrazolic chalcones, and allylic chalcones. Pharmacol Pharm. 2011, 2, 282–288.

5. Sivakumar, PM.; Prabhakar, PK.; Doble, M. Synthesis, anti-oxidant evaluation, and quantitative structure–activity relationship studies of chalcones. Med Chem Res. 2011, 20, 482–492.

6. Kamal, A.; Kashi Reddy, M.; Viswanath, A. The design and development of imidazothiazole-chalcone derivatives as potential anticancer drugs. Expert Opin Drug Discov. 2013, 8, 289–304.

7. Neves, MP.; Lima, RT.; Choosang, K.; Pakkong, P.; de São José Nascimento, M.; Vasconcelos, MH.; Pinto, M.; Silva, AM.; Cidade, H. Synthesis of a natural chalcone and its prenyl analogs—evaluation of tumor cell growth-inhibitory activities, and effects on cell cycle and apoptosis. Chem Biodivers. 2012, 9, 1133–1143.

8. Orlikova, B.; Tasdemir, D.; Golais, F.; Dicato, M.; Diederich, M. Dietary chalcones with chemopreventive and chemotherapeutic potential. Genes Nutr. 2011, 6, 125–147.

9. Ekhlass, N.; El-Badry, YA.; Eltoukhy, AMM.; Ayyad, RR. Synthesis and antiproliferative activity of 1-(4-(1H-Indol-3-Yl)-6-(4-Methoxyphenyl) pyrimidin-2-yl)hydrazine and its pyrazolo pyrimidine derivatives. Med Chem. 2016, 6, 4. doi:10.1186/s13065-018-0437-y

10. Lu, X.; Wan, B.; Franzblau, SG.; You, Q. Design, synthesis and antitubercular evaluation of new 2-acylated and 2-alkylated amino-5-(4-(benzyloxy)phenyl)thiophene-3-carboxylic acid derivatives. Part 1. Eur J Med Chem. 2011, 46, 3551–3563.

11. Kaushik, NK.; Kim, HS.; Chae, YJ. Synthesis and anticancer activity of di(3-thienyl)methanol and di(3-thienyl)methane. Molecules. 2012, 17, 11456–11468.

12. Shehab, WS.; Saad, HA.; Mouneir, SM. Synthesis and antitumor/antiviral evaluation of 6-thienyl-5-cyano-2-thiouracil derivatives and their thiogalactosides analogs. Curr Org Synth. 2017, 14, 291–298.

13. Frisch, MJ.; Trucks, GW.; Schlegel, HB.; Scuseria, GE.; Robb, MA.; Cheeseman, JR.; Scalmani, G.; Barone, V.; Petersson, GA.; Nakatsuji, H.; Li, X.; Caricato, M.; Marenich, AV.; Bloino, J.; Janesko, BG.; Gomperts, R.; Mennucci, B.; Hratchian, HP.; Ortiz, JV.; Izmaylov, AF.; Sonnenberg, JL. Gaussian 16, 2016.

14. Al-Hussaini, N.; Al-Dulaimi, W.; Al-Salahi, R. Computational Mechanistic Study of Oxidation Reactions of Alcohols. J Mol Model. 2020, 26, 12.

15. Al-Khatib, M.; Al-Jumaily, A.; Al-Zubaidi, T. Quantum Mechanical Calculations on the Reaction Pathways of Alkyl Hydroperoxides. Int J Quantum Chem. 2019, 119, e25872.

16. Al-Saadi, H.; Al-Hakim, S.; Al-Majid, K. Computational study of bimolecular decomposition mechanisms of amines. J Chem Phys. 2020, 152, 234105.

17. Lee, C.; Yang, W.; Parr, RG. Development of the Colle-Salvetti Correlation-Energy Formula into a Functional of the Electron Density. Phys Rev B. 1988, 37(2), 785. doi:10.1103/PhysRevB.37.785

18. Abd Al-Razaq, E.; Buttrus, N.; Al-Kattan, W.; Jbarah, AA.; Al-Amin, M. Reactions of Pd2+ and Pt2+ with pyrrolidinedithiocarbamate and cystine ligands: synthesis and DFT calculations. J Sulfur Chem. 2011, 32, 159–169.

19. Assefa, MK.; Devera, JL.; Brathwaite, AD.; Mosley, JD.; Duncan, MA. Vibrational scaling factors for transition metal carbonyls. Chem Phys Lett. 2015, 640, 175–179.

20. Cossi, M.; Barone, V. Time-dependent density functional theory for molecules in liquid solutions. J Chem Phys. 2001, 115, 4708–4717.

21. Lee, C.; Yang, W.; Parr, RG. Development of the Colle-Salvetti correlation-energy formula into a functional of the electron density. Phys Rev B. 1988, 37, 785–789.

22. Becke, AD. Density-functional thermochemistry. IV. A new dynamical correlation functional and implications for exact-exchange mixing. J Chem Phys. 1996, 104, 1040-1046.

23. Bauernschmitt, R.; Ahlrichs, R. Treatment of electronic excitations within the adiabatic approximation of time dependent density functional theory. Chem Phys Lett. 1996, 256, 454–464.

24. Runge, E.; Gross, EKU. Density-Functional Theory for Time-Dependent Systems. Phys Rev Lett. 1984, 52, 997–1000.

25. Petersilka, M.; Gossmann, UJ.; Gross, EKU. Excitation Energies from Time-Dependent Density-Functional Theory. Phys Rev Lett. 1996, 76, 1212–1215.

26. Shehab, WS.; Mouneir, SM. Design, synthesis, antimicrobial activity and anticancer screening of some new 1,3-thiazolidin-4-ones derivatives. Eur J Chem. 2015, 6, 157–162.

27. Jacob, J.; Prakash Kumar, B. Dual COX/LOX inhibition: screening and evaluation of effect of medicinal plants of Kerala as anti-inflammatory agents. Pharmacogn Phytochem. 2015, 3, 62–66.

28. Simone, RD.; Chini, MG.; Bruno, I.; Riccio, R. Benzimidazole-1,2,3-triazole hybrid molecules: synthesis and evaluation for anti-bacterial/antifungal activity. J Med Chem. 2011, 54, 1565–1575.

29. Khalil, NA.; Ahmed, EM.; Mohamed, KO.; Nissan, YM. Synthesis and biological evaluation of new pyrazolone–pyridazine conjugates as anti-inflammatory and analgesic agents. Bioorg Med Chem. 2014, 22, 2080–2089.

30. Lokwani, D.; Azad, R.; Sarkate, A.; Reddanna, P.; Shinde, D. Structure-based library design (SBLD) for new 1,4-dihydropyrimidine scaffold as simultaneous COX-1/COX-2 and 5-LOX inhibitors. Bioorg Med Chem. 2015, 23, 4533–4543.

31. Abdelgawad, MA.; Bakr, RB.; Azouz, AA. Novel pyrimidine-pyridine hybrids: synthesis, cyclooxygenase inhibition, anti-inflammatory activity and ulcerogenic liability. Bioorg Chem. 2018, 77, 339–348.

32. Kotb, ER.; Soliman, HA.; Morsy, EMH.; Abdelwahed, NAM. New pyridine and triazolopyridine derivatives: synthesis, antimicrobial and antioxidant evaluation. Acta Pol Pharm. 2017, 74, 861–872.

33. Mojarrab, M.; Soltani, R.; Aliabadi, A. Pyridine based chalcones: synthesis and evaluation of antioxidant activity of 1-phenyl-3-(pyridin-2-yl)prop-2-en-1-one derivatives. Jundishapur J Nat Pharm Prod. 2013, 8, 125–130.

34. Al-Rashid, FH.; Shafiq, Z.; Al-Mansour, R. Preparation, characterisation and biological activity studies for some mixed ligands complexes of 1,10-phenanthroline and Schiff base ligand with metal ions. Diyala J Pure Sci. 2017, 3, 150–161.

35. Al-Mansour, RK. Microwave preparation, spectral studies and antimicrobial activities evaluation of Mn(II), Ni(II), Hg(II), Co(II) and Cu(II) complexes with Schiff base ligand. IHJPAS. 2016, 30, 72–85.

36. Al-Mansour, RK.; Zaidan, B.; Al-Marsomy, NA. Synthesis, characterization and antibacterial activities of mixed ligand complexes of Schiff base derived from benzidine and 2-benzoyl benzoic acid. Diyala J Pure Sci. 2017, 13. DOI: 10.24237/djps.1303.189C

37. Karam, NH.; Tomma, JH.; Al-Dujaili, AH. Synthesis and characterisation of heterocyclic compounds derived from 4-hydroxy and 4-amino acetophenone. Ibn al-Haitham J Pure Appl Sci. 2013, 26, 296–312.

38. Al-Mansour, RK.; Ghanim, FH.; Shafiq, ZA. Preparation, characterisation and biological activity studies for some mixed ligands complexes of 1,10-phenanthroline and Schiff base ligand with metal ions. Diyala J Pure Sci. 2017. DOI: 10.24237/djps.1303.226C

39. Ibtisam, JD.; Waleed, M.; Al-Mansour, RK. Effect of different concentration and pH on complexes formation of new tetradentate Schiff base ligand. Res J Pharm Tech. 2019, 12(9), 4471–4479.